



Original Article

Design and Fabrication of an Active Knee Orthosis for Rehabilitation of Lower Limbs

Mohammad Amin Iravani Rad¹, MSc; Ali Mokhtarian^{1*}, PhD; Mohammad Taghi Karimi², PhD

¹Department of Mechanical Engineering, Islamic Azad University, Khomeinishahr Branch, Isfahan, Iran

²Orthotics and Prosthetics Department, School of Rehabilitation Sciences, Shiraz University of Medical Sciences, Shiraz, Iran

ARTICLE INFO

Article History:

Received: 08/12/2018

Revised: 17/02/2019

Accepted: 01/05/2019

Keywords:

Active orthosis

Rehabilitation

Lower extremities

Cerebrospinal injury

PID controller

Design and test

Arduino

Please cite this article as:

Iravani Rad MA, Mokhtarian A, Karimi MT. Design and Fabrication of an Active Knee Orthosis for Rehabilitation of Lower Limbs.

JRSR. 2019;6(3):109-116. doi: 10.30476/jr.sr.2019.75405.

ABSTRACT

Background: The main objective of this study is to design and produce a two-link active knee orthosis with 2 degrees of freedom to rehabilitate patients' lower extremities in moving their feet. This study aimed to provide motor independence in patients with cerebrospinal cord injury, quadriceps and knee joint injuries in athletes, and deviation of the quadriceps angle in the elderly.

Methods: The current research is an experimental method. We have tried, while eliminating a physiotherapist, to enable movement modification of organs that suffer from dynamics poverty and ensure an improved movement for injured organs. In order to reduce external fluctuations and turbulences and determine orthosis opening and closing angle, a DC motor with a helical gearbox and a PID controller was used. In addition, an Arduino microcontroller and a potentiometer were used for processing and angle determination, respectively, to provide minimum wiring and maximum accuracy and performance for the proposed orthosis.

Results: In order to verify the mechanical parts of the proposed orthosis, three tests were performed with different angles without charging the orthosis.

Conclusion: Results showed that the proposed orthosis admissibly tracked intended angles and had a proper weight and volume to provide safety and comfort for the foot and knee joint.

2019© The Authors. Published by JRSR. All rights reserved.

Introduction

With advances in both mechatronics and biomedical engineering, new robotic systems have been created while others have been optimized or updated based on our needs. As an example of such technologies in biomedical engineering, technical orthopedics and rehabilitation are exceedingly dependent on other fields of science, mechatronics in the design, fabrication, and optimization of rehabilitation orthoses for patients. Cerebrospinal, quadriceps, or knee injuries (in athletes) and age-associated deviation of the quadriceps muscle

angle (Q-angle) are all among the most important causes of mobility impairment that may lead to balance disorders and limb paralysis, as well as the risk of fatality.

Spinal injuries are either traumatic or non-traumatic. Trauma accounts for 70% of all such injuries. Blunt spinal cord trauma can lead to spinal cord injuries due to fracture, vertebral dislocation, or a combination of both (fracture–dislocation). Non-traumatic injuries account for the remaining 30% of the spinal cord injuries, and is often a result of certain diseases or vascular disorders [1].

Cerebral injuries, too, can cause mobility disorders in patients. They increase the risk of death of the damaged brain cells that control the movement of limbs. Unfortunately, a final cure is yet to be presented for the death of brain cells which often puts the mobility independence of patients at risk. The cells, remaining

*Corresponding author: Ali Mokhtarian, Department of Mechanical Engineering, Islamic Azad University, Khomeinishahr Branch, Isfahan, Iran. Tel: +98 913 3129673

Email: alimokhtarian@gmail.com

unharmful, can partially assume the control of the limbs that the dead cerebral cells were in charge of [2].

With more people taking part in competitive and recreational athletic activities, quadriceps muscle and knee joint injuries have risen considerably, exacting economic, motivational, and mental costs on sports clubs and athletes alike. Furthermore, anterior cruciate ligament injuries are common causes of acute or chronic knee pain. The quadriceps femoris is a group of four muscles including the rectus femoris. The most common damages to the muscle involve contusion and strain that often affects the rectus femoris which is situated at the front of the thigh. Other damage to the muscle may include tendon strain, separation, or rupture, partial or a complete tear of a strained muscle, and rupture of the fascia that are symptomized by swelling in the form of subcutaneous bulges [3].

The aging Q-angle deviation is a condition which is experienced by almost all individuals of all ages. Knee pain can have different causes some of which are treatable (*i.e.*, infection, Q-angle deviation, patellar malalignment, and ligament strain) while others are not (*i.e.*, osteoarthritis). If not diagnosed and treated at the early stages, knee pain can develop into a complication with no definitive treatment or requiring a demanding surgery. A common cause of knee pain is the Q-angle deviation which often begins in adolescence and, if not treated accordingly, exacerbates over time with several complications, some of them irreversible [4].

In recent years, many studies have attempted to develop different rehabilitation exoskeletons, and much progress has been made. Based on their mechanism and rehabilitation principles, lower limb rehabilitation exoskeletons can be divided into four categories [5] namely, treadmill-based exoskeletons (*e.g.*, LOPES [6] and ALEX [7]), leg orthosis and exoskeletons (*e.g.*, KAFO [8] and HAL [9]), footplate-based end-effector devices (*e.g.*, Haptic Walker [10]), and platform-based end-effector robots (*e.g.*, ARBOT [11]). Samer Mohammed *et al.* addressed the knee joint control for rehabilitation and support purposes based on a nonlinear observer to evaluate the muscular torque developed by the patient [12]. In another study, Samer Mohammed *et al.* presented a method to ensure the compensation of the damping and gravity effects of the wearer's (patient's) leg to control and reduce the swinging. Furthermore, the activity of the knee muscles was measured by electromyography. The results revealed that the device efficiently reduces the muscular activity required to perform the same flexion–extension movements [13]. Pott *et al.* designed a knee orthosis to determine the fractional external torque, as well as to support the knee against pressure from biomechanical loads, that reduced the stress on foot muscles when standing [14]. Long *et al.* adopted a disturbance rejection control-based strategy simulating the human gait for lower limb rehabilitation. Their experimental results are suggestive of the better performance of the disturbance rejection control than PID control [15].

The current study aims to design and produce an

active knee orthosis to help athletes who suffer from cerebrospinal, quadriceps, and knee joint injuries as well as older people with a deviated Quadriceps femoris angle, such that the patients can keep their balance and avoid turmoil while walking.

Methods

Dynamic Model

In this experimental method, a DC motor with a helical gearbox is used to minimize the volume, which is of a great importance for an orthosis. A PID controller is utilized to control the angle and torque of the motor, which was designed by MATLAB and Simulink and applied to Arduino microcontroller to increase processing accuracy and speed as well as minimize wiring and orthosis volumes so the patient could use it everywhere without a nurse's help. Moreover, instead of using an encoder sensor to determine orthosis angle for knee joint which leads to an increased weight, and volume, a potentiometer is used as an innovation in orthosis production. SolidWorks modeling and simulation is utilized to design and analyze orthosis movement. It should be noted that a prototype of the proposed orthosis was designed and produced, on which three tests were performed by applying different angles to verify mechatronic parts of the orthosis. Results show that the proposed orthosis has a permissible weight and volume, which is an important factor for a patient's foot. In addition, after applying intended angles, a proper response was received from the orthosis and mechanical and electrical parts, as well as PID controller, showing appropriate coordination and performance.

A 2DOF system was designed and simulated according to Figure 1. The system is driven by an electric motor and comprises of two rods of the weights m_1 and m_2 and end-to-end lengths of l_1 and l_2 . Moreover, their respective centers of mass are located at l_{c1} and l_{c2} from the origin (Table 1). The system was studied with two degrees of freedom, namely q_1 and q_2 . Figure 1 illustrates a schematic view of the studied system.

Now, we discuss the process of obtaining dynamic equations. The Lagrange multipliers were employed to solve the system (Eq. 1).

$$\frac{d}{dt} \left(\frac{\partial L}{\partial \dot{q}_i} \right) - \frac{\partial L}{\partial q_i} = Q_i \quad i = 1, 2, \dots, N \quad (1)$$

Considering the external forces exerted on the 2DOF system, the Lagrange equations were written as presented in Eqs. 2 and 3.

$$\frac{d}{dt} \left(\frac{\partial L}{\partial \dot{q}_1} \right) - \frac{\partial L}{\partial q_1} = Q_1 \quad (2)$$

$$\frac{d}{dt} \left(\frac{\partial L}{\partial \dot{q}_2} \right) - \frac{\partial L}{\partial q_2} = Q_2 \quad (3)$$

Now, by obtaining the kinetic and potential energies and

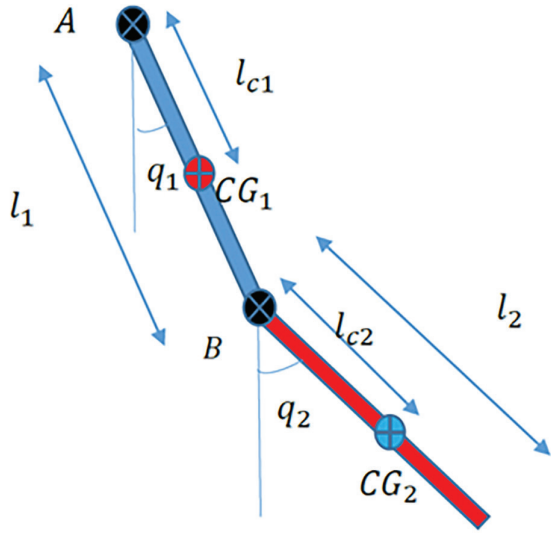


Figure 1: The dynamic model of the simulated system

Table 1: Parameters of the simulated dynamic model of the system

The weight of the first link	m_1
The weight of the second link	m_2
The end-to-end length of the first link	l_1
The end-to-end length of the second link	l_2
Distance from the origin to the center of mass of the first link	l_{c1}
Distance from the origin to the center of mass of the second link	l_{c2}
The angle of rotation of the first link	q_1
The angle of rotation of the second link	q_2
External torque applied to the first link	τ_1
External torque applied to the second link	τ_2
Origin	A
The connection of the links	B
The center of mass of the first link	CG ₁
The center of mass of the second link	CG ₂
The moment of inertia of the first link	I_1
The moment of inertia of the second link	I_2

substituting them in Eq. 4, the Lagrange value is obtained.

$$L = T - U \quad (4)$$

According to Eqs. 2 and 3, the potential and kinetic energies of the system must be first calculated. Therefore, in the following, the overall system potential energy is obtained—which is the sum of the potential energies of the two rods.

$$U = -m_1 l_{c1} \cos(q_1(t)) g + m_2 (-l_1 \cos(q_1(t)) - l_{c2} \cos(q_2(t))) g \quad (5)$$

Next, the overall kinetic energy of the system is obtained—which is the sum of the kinetic energies of the two rods.

$$T = \sum \frac{1}{2} m_i v_{CGi} \cdot v_{CGi} + \frac{1}{2} I_i \dot{\theta}_i^2 \quad (6)$$

Now the Lagrange equation can be calculated (Eqs. 8 and 9).

The dynamic system equations were obtained. To simulate said equations by MATLAB, numerical data, including parameters and initial values, are needed.

The length and mass specifications of the wearer's limbs are constant in the equations of motion and must be calculated for each wearer separately. The required wearer's anthropometric data can be estimated based on the height and body mass of each wearer using the equations found in Table 2 [16]. Furthermore, Table 2 equations are listed in Table 3.

Table 2: Anthropometric Calculation Parameters

1	$g = 9.81 \text{ m/s}^2$
2	$m_1 = 5 \text{ kg}$
3	$m_2 = 0.061M$
4	$m_2 = 0.100M$
5	$L_s = 0.245h$
6	$L_{sh} = 0.285h$
7	$L_{c1} = 0.5L_1$
8	$L_{c2} = L_2 - 0.606L_{sh}$
9	$L_{c2} = 0.433L_2$
10	$I_1 = \frac{1}{12} m_1 L_1^2$
11	$I_2 = m_2 (0.416L_{sh})^2$
12	$I_2 = m_2 (0.323L_2)^2$

$$T = \quad (7)$$

$$\begin{aligned} & 1/2 (\dot{q}_1(t))^2 (m_1 l_{c1}^2 + I_1) + \\ & \cos(q_1(t)) (\dot{q}_1(t)) (\dot{q}_2(t)) \cos(q_2(t)) l_1 l_{c2} m_2 + \\ & 1/2 (\dot{q}_1(t))^2 l_1^2 m_2 + (\dot{q}_1(t)) \sin(q_1(t)) (\dot{q}_2(t)) \sin(q_2(t)) l_1 l_{c2} m_2 + 1/2 (\dot{q}_2(t))^2 l_{c2}^2 m_2 + 1/2 I_2 (\dot{q}_2(t))^2 \end{aligned}$$

$$\begin{aligned} i = 1: & (\ddot{q}_1(t)) m_1 l_{c1}^2 + I_1 \ddot{q}_1(t) + m_2 l_1 \cos(q_1(t)) l_{c2} \cos(q_2(t)) \ddot{q}_2(t) - m_2 l_1 \cos(q_1(t)) l_{c2} \sin(q_2(t)) (\dot{q}_2(t))^2 + \\ & (\ddot{q}_1(t)) l_1^2 m_2 + \\ & \sin(q_1(t)) (\ddot{q}_2(t)) \sin(q_2(t)) l_1 l_{c2} m_2 + \sin(q_1(t)) (\dot{q}_2(t))^2 \cos(q_2(t)) l_1 l_{c2} m_2 + m_1 l_{c1} \sin(q_1(t)) g + \\ & m_2 l_1 \sin(q_1(t)) g = \tau_1 - \tau_2 \end{aligned} \quad (8)$$

$$\begin{aligned} i = 2: & \\ & -m_2 l_{c2} \cos(q_2(t)) l_1 \sin(q_1(t)) (\dot{q}_1(t))^2 + \\ & m_2 l_{c2} \cos(q_2(t)) l_1 \cos(q_1(t)) \ddot{q}_1(t) + \\ & (\ddot{q}_1(t)) \sin(q_1(t)) \sin(q_2(t)) l_1 l_{c2} m_2 + (\dot{q}_1(t))^2 \cos(q_1(t)) \sin(q_2(t)) l_1 l_{c2} m_2 + (\ddot{q}_2(t)) l_{c2}^2 m_2 + I_2 \ddot{q}_2(t) + \\ & m_2 l_{c2} \sin(q_2(t)) g = \tau_2 \end{aligned} \quad (9)$$

Simulation of the Equations and Determining the Joints Torque

Here, the mass and geometry specifications of the wearers' lower limbs are estimated as a fraction of the height and total weight of the person based on Table 1 and other body measurement tables [16]. Maple and MATLAB were employed to simulate the equations. By an inverse dynamics solution and applying the different hip and knee joint angles (q_1 & q_2) and their derivatives to the equations of motion (Eqs. 8 and 9), the knee joint torque can be obtained as illustrated in Figure 2.

Moreover, the power required to create motion in the knee joint is demonstrated in Figure 3.

According to Figures 2 and 3, a maximum torque of 20 Nm is required at the knee joint, which means the incorporated motor must provide a larger torque than that. To this end, a suitable motor capable of a higher torque was selected.

Results

The external active orthosis consists of general sectors of mechanical, electrical, and control. In the mechanical sector, at first, parts are designed by the SolidWorks software program (Figure 4). Then, using fiber carbon alloy, the parts are produced, which consist of a joint with

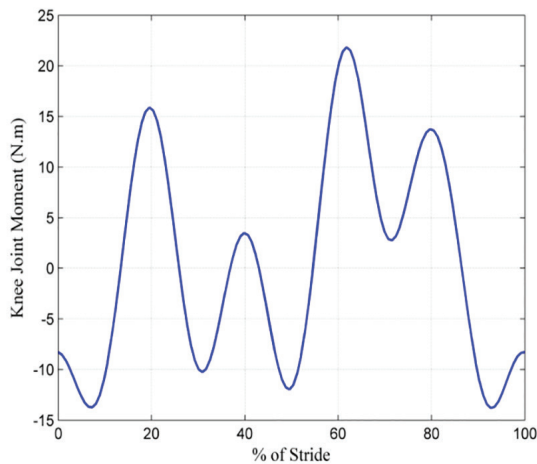


Figure 2: The knee joint torque diagram

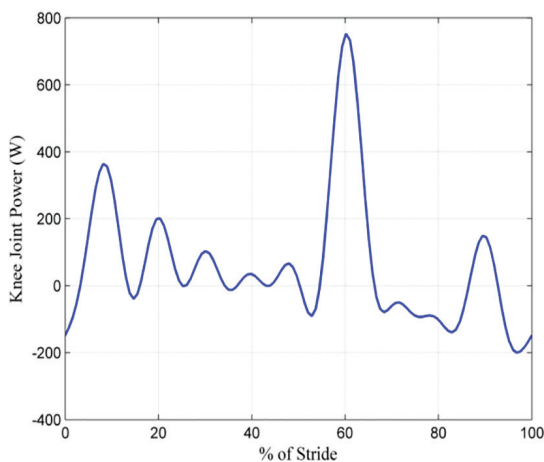


Figure 3: Power required for creating motion in the knee joint

Table 3: Symbol Index

Gravitational acceleration on earth (ms^{-2})	g
Total wearer's body mass (kg)	M
The actuator arm weight (kg)	m_1
Total weight of the shank (kg)	m_2
The weight of the thigh (kg)	m_3
Wearer's height (m)	h
Length of the link between the motor and the patient's leg (m)	L_1
The distance between the knee joint and the connection of the driver motor link to the shank (m)	L_2
Length of the thigh (m)	L_3
Length of the leg (m)	L_{3h}
The distance between the center of mass of the actuator and its connection to the shaft (m)	L_{c1}
The distance from the center of mass of the shank and foot system to the connection of the actuator arm to the shank (m)	L_{c2}
The distance between the center of mass of the thigh and the hip joint (m)	L_{c3}
The moment of inertia of the actuator arm around its center of mass (kgm^2)	I_1
The moment of inertia of the whole shank and foot around its center of mass (kgm^2)	I_2
The moment of inertia of the thigh around its center of mass (kgm^2)	I_3

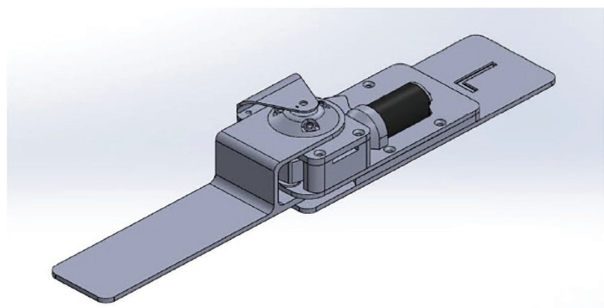


Figure 4: Knee Orthosis Designing in SolidWorks



Figure 5: Adaptable Cuffs

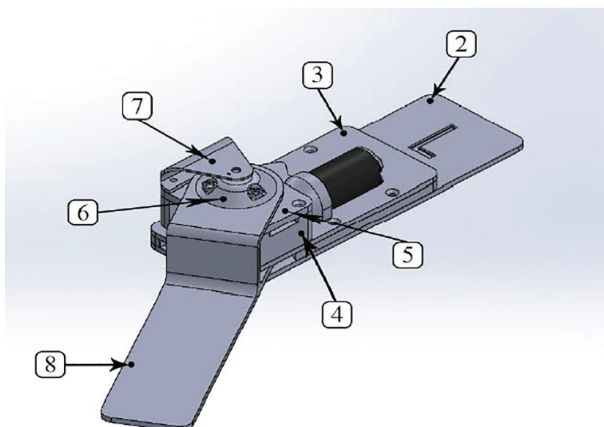


Figure 6: Different Parts of the Knee Orthosis

a degree of freedom, a DC motor with a helical gearbox, two arms to connect to the thighs and legs as well as two adaptable cuffs to perfectly connect the orthosis to legs and thighs. Mechanical sector of the orthosis, the main function of which is to connect to the patient's foot and apply movement up to 60 degrees, consists of various parts that are (Figure 5) and (Figure 6):

1. Adaptable cuffs
2. An arm connected to the thigh with a proper angle controller for the patient's clinical safety
3. A part holding the motor and a support for the moving arm connected to the leg
4. A part holding the shaft link
5. A part holding linker connecting the shaft to the motor
6. A base holding the sensor
7. A moving arm connected to the leg

Adaptable cuffs are a part of the orthosis that are directly connected to the patient's body. The cuffs are placed on shanks and legs and are responsible for applying movement to the patient's foot. Thus, they are required to be connected to the patient's leg with no unwanted slackness. An advantage of these cuffs is their adaptability for people of different sizes. The cuffs material is a fabric of an available type with high durability and low price, providing comfort and a low volume for people using it. It is worth noting that, for the patients' comfort when using right and left foot orthosis, a belt is designed that connects the cuffs around the patient's waist, reducing orthosis weight and eliminating slackness while moving.

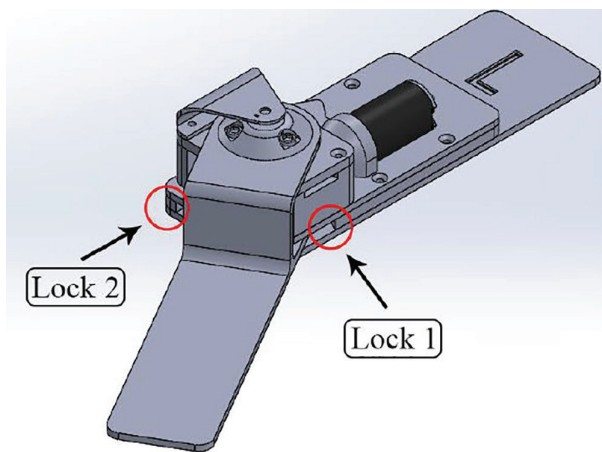


Figure 7: Locks Positions on the Designed Orthosis

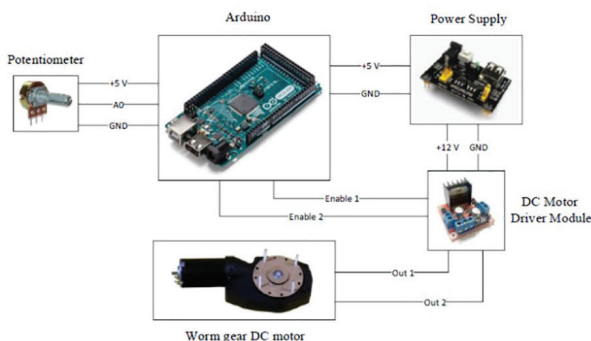


Figure 8: Implementation of Knee Orthosis Electrical Sector

In the mechanical design, in order to provide a maximum safety for the patents' feet, two locks are used and the opening and closing angle of the orthosis is restricted in the range of 0-65 degrees. The locks (Figure 7) prevent unpredictable events and minimize error possibility.

Electrical and control sector of the orthosis consists of a dynamic model of the motor, driver, Arduino, and sensor to control motor motions.

Figure 8 shows the hardware connection of the orthosis and used parts.

As can be seen in Figure 8, a power module is used to supply a voltage of Arduino and DC motor driver. The voltage required to start these two modules are 5 and 12 V DC, respectively.

A volume potentiometer is used as an analog sensor which is connected to the base of Arduino board analog. In order to start the driver module of the motor, after supplying 12 V DC, Enable 1 and Enable 2 have to be activated. For this purpose, PWM digital bases of an Arduino board are used. After the motor driver has been activated, Out 1 and Out 2 bases of motor starting voltage are moved to helical gearbox motor and it is started. For the sensor used here, it should be noted that the use of the encoder sensor increases orthosis weight and volume as well as controller design complication. Thus, for a design innovation, mechanical design complication reduction, and weight reduction which is of great importance in rehabilitation, a 10 KΩ volume potentiometer is used instead of an encoder sensor [17].



Figure 9: Assembled Parts Holding the Sensor with a Volume Potentiometer

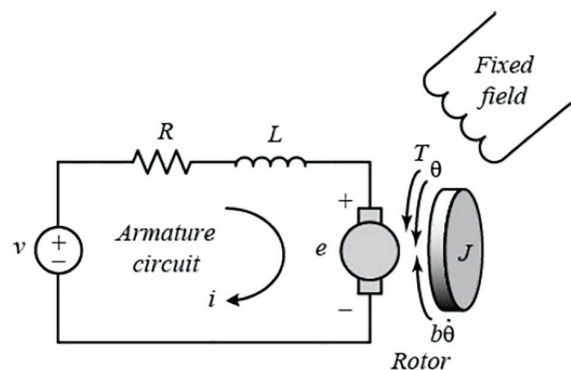


Figure 10: Armature Electrical Circuit and Rotor Field Diagram [18]

The only downside of the proposed orthosis is its noise capture. In order to eliminate this drawback, a 100 nF capacitor is used parallel to the potentiometer to filter the noise. Figure 9 represents a potentiometer installed on the sensor holding part.

In order to design an orthosis controller, DC motor is modeled by MATLAB. The DC motor is a coupled electromechanical system consisting of two sectors: electrical and mechanical. Figure 10 shows the armature electrical circuit and the rotor field diagram [18].

A system with two degrees of freedom was used to control the DC motor. As can be seen in Figure 10, the electrical circuit is a RL series circuit where electromagnetic force is converted into rotational mechanical force by Converter J. Equations governing the DC motor are as follows [19]:

$$T = K_t i \quad (10)$$

Where T is motor torque, K_t is armature current-dependent constant coefficient, and i is armature current.

$$e = K_e \dot{\theta} = K_e \omega \quad (11)$$

In which e is electronic magnetic force (EMF), K_e is motor constant coefficient, and $\dot{\theta}$ is gearbox angular velocity. In SI, armature constant K_t equals to motor constant K_e . Using relations (10) and (11), an electromechanical coupling is done. Using Figure 10 and a combination of Newton's and Kirchoff's laws, relation (12) is achieved as:

$$\begin{cases} J\ddot{\theta} + b\dot{\theta} = K_t i & (12) \\ L\frac{di}{dt} + Ri = V - K_e \dot{\theta} \end{cases}$$

According to Figure 10 and relation (12), a first-order equation and a second-order equation are obtained for electronic and mechanical sectors, respectively. In the mechanical equation, $J\ddot{\theta}$ is rotational inertia, while $b\dot{\theta}$ is rotational friction. In electronic equation, $L\frac{di}{dt}$ is the potential difference between the two ends of the inductor, while Ri is the voltage of the two ends of the resistor which equals to the difference of input voltage V and the two ends voltage e .

For simplicity of modeling, design, and implementation of the controller, using MATLAB Simulink and system identification toolbox, the motor is modeled and implemented in a controlled environment.

Design and Simulation of the Control Strategy for the Rehabilitation Robotic Exoskeleton

The PID controller is one of the most common examples of the feedback control algorithm which is applicable in several control processes, including DC motor speed control, pressure control, and temperature control. The PID controller calculates the "error" between the process output and the desired input. The controller is intended to minimize the error by adjusting process control inputs. The PID controller is composed of Proportional, Integral, and Derivative components, each of which receives the error signal as input and provides an output for summation. The output of the controller is that of the three components and is supplied to the system for correcting the error. The standard PID controller equation is presented by Eq. 13.

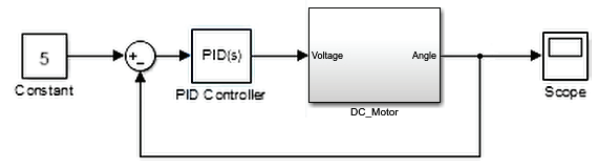


Figure 11: The knee orthosis controller model

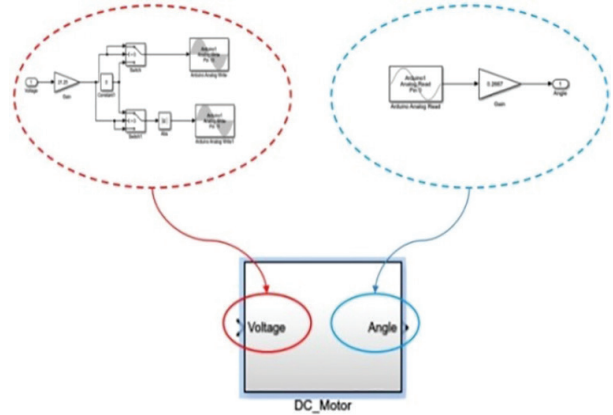


Figure 12: The modeled DC motor block input and output

$$output(t) = K_p \left(e(t) + \frac{1}{T_i} \int_0^t e(T) dT + T_d \frac{de}{dt} \right) \quad (13)$$

Therefore, the conversion function of a PID controller is obtained in the form of Eq. 14.

$$G(s) = K_p + \frac{K_i}{s} + K_d s \quad (14)$$

The PID control system was implemented in the Simulink environment, in MATLAB (Figures 11 and 12). In the designed DC_Motor block, the input and output serve for controlling the angle and speed of the DC motor.

The signal $u(t)$, the PID controller output, is calculated as a ratio of the current error in the system (the current performance), added to the sum of system errors (previous performance), added to the differentiated current error (a linear estimation of the future error) and then applied to the system for error correction.

Furthermore, parameters K_p , T_i , and T_d can be tuned by such well-known methods as the transfer function, although in practice, they can be accurately approximated based on observations of the system. The Ziegler–Nichols method is a well-known, experimental method

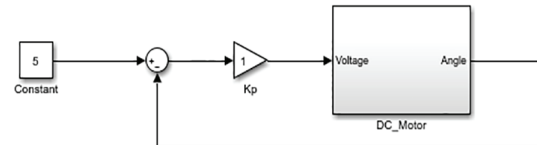


Figure 13: Implementation of the Closed-Loop Method

Table 4: Ziegler–Nichols [21]

K_u	K_i	K_p	Type of Controller
-	-	$0.5 K_u$	P
-	$1.2 K_p / T_u$	$K_u / 2.2$	PI
$K_p T_u / 8$	$2 K_p / T_u$	$0.6 K_u$	PID

for determining PID parameters. In 1942, Ziegler and Nichols proposed the closed- and open-loop methods for tuning PID controllers [20, 21].

In the closed-loop method addressed here, first, the derivative and integral blocks are separated from the circuit, leaving only the proportional one (Figure 13). In theory, eliminating the other control agents means assuming T_i to be infinite and T_d to be zero. The set point was then applied incrementally from small K_p values until oscillation was found in the output diagram. In this case, the period of the oscillation is denominated T_u and the oscillator gain K_u . Accordingly, PID parameters were obtained as listed in Table 4.

The proportional gain started at 0.01 and the system was in full oscillation at 20 (Figure 14).

According to Figure 14, T_u and K_u are 0.16 and 20, respectively. PID values are obtained by substituting these parameters in Table 4 and then in the Function Block Parameters: PID Controller in MATLAB.

The response of the system integrating the PID controller after applying angles (55° and 0°) is illustrated in Figure 15.

Discussion

In this section, we describe the steps of the experiment on how the orthosis functions and how electronic

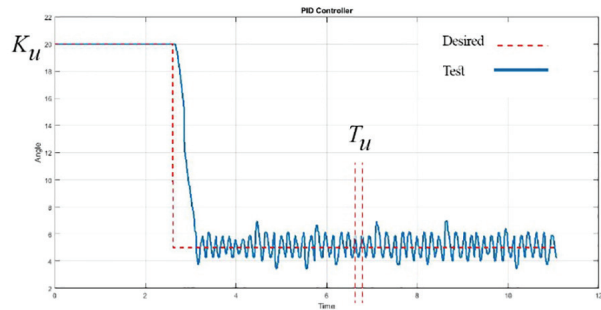


Figure 14: PID Controller Design

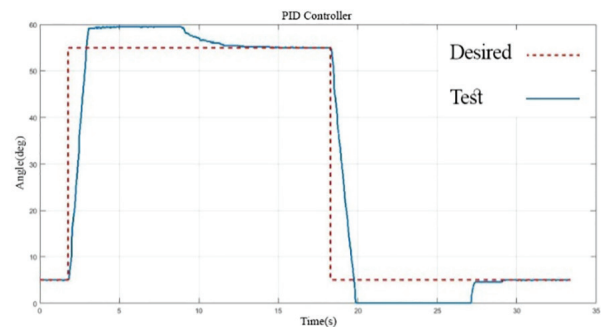


Figure 15: The response of the system integrating the PID controller

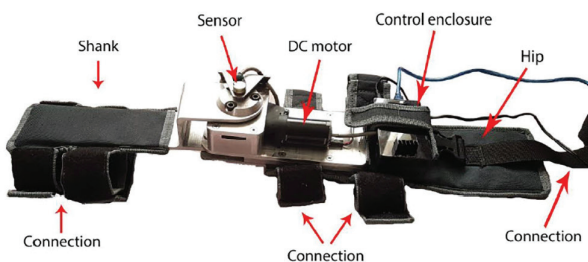


Figure 16: Experimental Platform

and mechanical parts cooperate with each other as well as investigate the performance of the controller implemented on the microcontroller. The active orthosis, or in other words, the mechatronic robot is capable of controlling and rotating in the range of 0-60 degrees. The real experimental platform is shown in Figure 16.

Three tests of verification, feasibility, and exoskeleton were performed on the proposed orthosis.

The proposed orthosis is a prototype and the tests were done without applying a charge to properly investigate the designed controller performance while verifying all assembled electronic and mechanical parts of the

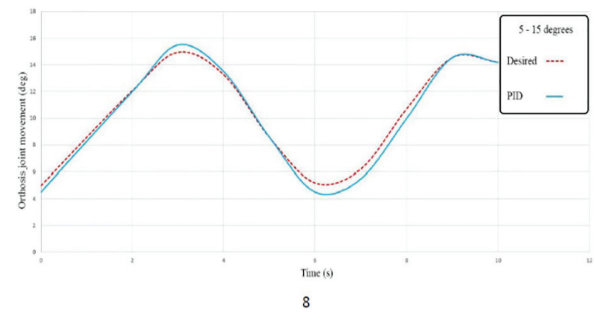


Figure 17: System Response for Degrees of 5 and 15

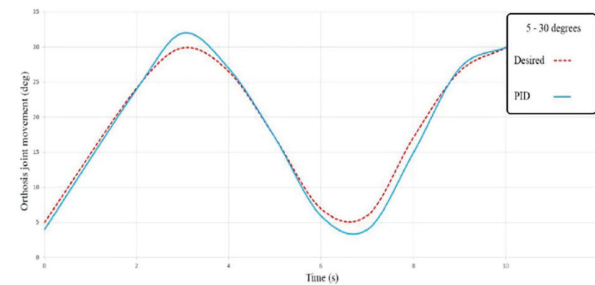


Figure 18: System Response for Degrees of 5 and 30

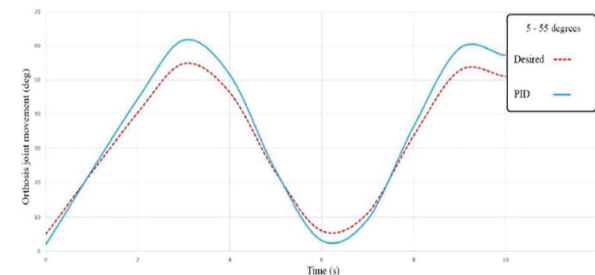


Figure 19: System Response for Degrees of 5 and 55

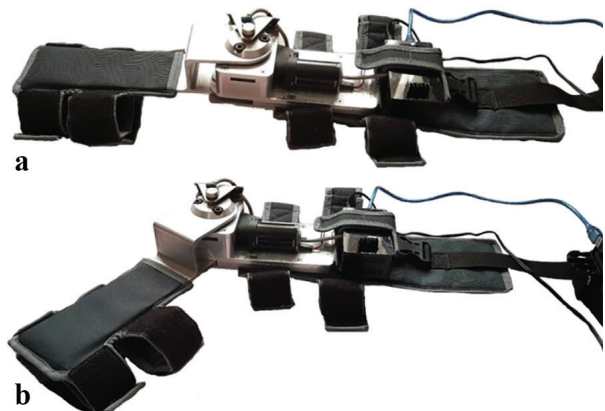


Figure 20: System Response for Degrees of 5 (a) and 55 (b) without applying load

orthosis. For this purpose, different angles were applied. It should be noted that the tests were real-time.

In the tests, degrees of 5 and 15, 5 and 30, and 5 and 55 were applied to the designed PID controller in MATLAB. Figures 17, 18, and 19 show the responses that admissibly tracked intended angles of the controller.

Figure 20 demonstrates system responses for 5 and 55 cases on the proposed orthosis (without applying load).

Conclusion

A simple mechanical and almost electronic structure of the proposed system shows that mechanical and electronic parts design and assembly and coupling them coordinates with a good performance, and there was no problem when using it. In addition, the use of a potentiometer as a sensor to determine the angle for the orthosis joint, which was an innovation, was followed by an accurate response in determining intended angles, helping in reducing weight and volume as well as simplifying the rehabilitation orthosis programming. On the other hand, the use of a DC motor with a helical gearbox provided the intended torque as well as helping in orthosis weight and volume reduction.

All of the above, including the electronic and mechanical sector that attempted to minimize the rehabilitation orthosis weight and volume, will provide great assistance in detecting and eliminating possible failures. A PID controller was utilized to control the orthosis so intended rotation range would be determined. In addition to locks embedded in orthosis, the controller limits the orthosis joint opening and closing range to provide safety for patients' feet. Three tests were performed to verify the coordination of electronic, mechanical, and control sector of the proposed orthosis, where various angles were applied. The tests showed that electronic and mechanical parts coordinated well and the PID controller admissibly tracked the intended angles. Finally, it should be noted that the proposed orthosis shows great potential to be used for the rehabilitation of patients' feet with other optimized controllers.

Acknowledgment

The authors express their appreciation to Dr. Ali Mokhtarian (Department of Mechanical Engineering, Islamic Azad University, Khomeinishahr Branch, Isfahan, Iran) for his helpful comments on this paper. We also thank Dr. Mohammad Taghi Karimi (Orthotics and Prosthetics Department, School of Rehabilitation Sciences, Shiraz University of Medical Sciences, Shiraz, Iran) for his help and support.

Conflict of interest: None declared.

References

1. Ebrahim B, Structure and Function of the Neuromuscular System, supervised by Dr. Hasan Ashayeri in association with Mosayyeb Barzekar, 1st Edition, Spring 2006.
2. Akbar S, Neuromuscular Diseases, Jafari Publications, 2nd Edition, Spring 1997.
3. Shafipour A., "The comparison of knee joint position sense in soccer player, volleyball player and non-athlete men.," J Shahrekord Univ Med Sci, 2014;16(3):33-42.
4. Hamidreza A, Mohammad F, "An Investigation of the Relationship between the Quadriceps Muscle Angle and Knee Pain.," J Shahrekord Univ Med Sci, 2012;14(1):11-19.
5. Long Y, Du Z-j, Wang W, Dong W., "Development of a wearable exoskeleton rehabilitation system based on hybrid control mode.," IJARS, 2016;13(5):1-10.
6. Veneman JF, Kruidhof R, Hekman EE, et al., "Design and evaluation of the LOPES exoskeleton robot for interactive gait rehabilitation.," IEEE TNS and RE, 2007;15(3):379-386.
7. Banala SK, Sai K., Seok Hun Kim, Sunil K. Agrawal, and John P. Scholz., "Robot assisted gait training with active leg exoskeleton (ALEX).," In 2008 2nd IEEE RAS & EMBS ICBR and Biomecha, 2008:653-658.
8. Sawicki GS, Ferris DP., "A pneumatically powered knee-ankle-foot orthosis (KAFO) with myoelectric activation and inhibition.," J neuro and rehab, 2009;6(1):6-23.
9. Sankai, Yoshiyuki., "HAL: Hybrid assistive limb based on cybernics", Robo Res, 2007;(66):25-34.
10. Stefan H, Henning S, Cordula W., "Upper and lower extremity robotic devices for rehabilitation and for studying motor control.," CON, 2003;16(6):705-710.
11. Saglia J, Tsagarakis NG, Dai JS., "Control strategies for patient-assisted training using the Ankle Rehabilitation Robot (ARBOT).," IEEE/ASME TM, 2012;18(6):1799-1808.
12. Mohammed S, Huo W, Huang J, Rifai H, Amirat Y., "Nonlinear disturbance observer based sliding mode control of a human-driven knee joint orthosis.," Robo and Auto Sys, 2016;(75):41-9.
13. Huo W, Mohammed S, Amirat Y., "Walking Assistance Through Impedance Control of a Lower-Limb Exoskeleton.," CC and ERN II, 2017;(15):711-715.
14. Pott, P.P., Wolf, S.I., Block, J., van Drongelen, S., Grün, M., Heitzmann, D.W., Hielscher, J., Horn, A., Müller, R., Rettig, O., Konigorski, U., "Knee-ankle-foot orthosis with powered knee for support in the elderly", Proc. Inst. Mech. Eng. Part H J. Eng. Med., 2017;231(8):715-727.
15. Long Y, Du Z, Cong L, Wang W, Zhang Z, Dong W, "Active disturbance rejection control based human gait tracking for lower extremity rehabilitation exoskeleton.," ISA transactions, 2017;(67):389-397.
16. Winter DA. Biomechanics and motor control of human movement: John Wiley & Sons; 2009.
17. J. L. Harmse, "Motorcycle Data Acquisition System", 2010:1-36.
18. Salim, Jyoti Ohri., "Fuzzy based pid controller for speed control of dc motor using labview.," WSEAS transaction, 2015;(10):154-159.
19. Z. Y. Zhao, M. Tomizuka, and S. Isaka, "Fuzzy Gain Scheduling of PID Controllers", IEEE Trans. Syst. Man Cybern., 1993;23(5):1392-1398.
20. K. H. Ang, G. Chong, and Y. Li, "PID control system analysis, design, and technology", IEEE Trans. Control Syst. Technol., 2005;13(4):559-576.
21. D. Valério and J. S. da Costa, "Ziegler-Nichols type tuning rules for fractional PID controllers", Proc. IDETC, 2005:1431-40.